

# Mössbauer Investigation of $\gamma$ -Fe<sub>2</sub>O<sub>3</sub> Nanocrystals in Silica Matrix Prepared by the Sol-gel Method

C. Cannas, G. Concas<sup>a</sup>, F. Congiu<sup>a</sup>, A. Musinu, G. Piccaluga, and G. Spano<sup>a</sup>

Dipartimento di Scienze Chimiche, Università di Cagliari,  
S.P. Monserrato-Sestu Km 0.700, I-09042 Monserrato (Cagliari), Italy

<sup>a</sup> Dipartimento di Fisica, Università di Cagliari, and Istituto Nazionale per la Fisica della Materia,  
S.P. Monserrato-Sestu Km 0.700, I-09042 Monserrato (Cagliari), Italy

Reprint requests to Dr. F. C.; Fax: +39 070 510171, E-mail: franco.congiu@dsf.unica.it

Z. Naturforsch. **57 a**, 154–158 (2002); received January 14, 2002

A series of Fe<sub>2</sub>O<sub>3</sub>-SiO<sub>2</sub> nanocomposites (25 weight % of Fe<sub>2</sub>O<sub>3</sub>) has been prepared using a sol-gel method. Samples showing different features were obtained by varying the evaporation conditions acting on the surface / volume ratio of the starting sol. The samples were investigated using Mössbauer spectroscopy at low temperature. The Fe<sub>2</sub>O<sub>3</sub> nanoparticles have been identified as maghemite ( $\gamma$ -Fe<sub>2</sub>O<sub>3</sub>) particles. The samples show a superparamagnetic behavior with a blocking temperature that depends on the average particle size.

*Key words:* Nanostructures; Oxides; Sol-gel Growth; Mössbauer Spectroscopy;  
Magnetic Properties.

## 1. Introduction

Maghemite ( $\gamma$ -Fe<sub>2</sub>O<sub>3</sub>) is widely used in magnetic recording systems and catalysis [1, 2]. Its properties are enhanced when the size of the particles reaches the nanometer range [3, 4]. Nanosized  $\gamma$ -Fe<sub>2</sub>O<sub>3</sub> transforms to  $\alpha$ -Fe<sub>2</sub>O<sub>3</sub> (hematite) at rather low temperatures ( $\sim 350$  °C) [5, 6], but it can be stabilized by incorporating the nanoparticles into polymeric, glassy or ceramic matrices [5, 7, 8]. Moreover, a growing attention has recently been devoted to maghemite nanoparticles dispersed in a transparent matrix for their use in magneto-optical recording systems [7, 9, 10]. Among the various preparation procedures which can be used to obtain Fe<sub>2</sub>O<sub>3</sub>-SiO<sub>2</sub> nanocomposites, the sol-gel method has proven to offer some interesting features that allow controlling the final properties of the material [11, 12]. Several preparation methods have been tested, and some of them have proven to fulfill the requirement of producing selectively the  $\gamma$ -Fe<sub>2</sub>O<sub>3</sub> phase [7, 12]. It is difficult, however, to find a way of tailoring the particle size and regulating the connected physical properties.

Studies of the particle formation mechanism evidenced that the surface area and porosity are the main

factors affecting the particle growth [11]. Therefore we decided to prepare the Fe<sub>2</sub>O<sub>3</sub> / SiO<sub>2</sub> nanocomposites by a sol-gel method similar to the one successfully used by del Monte et al. [12], but varying the evaporation conditions (and as a consequence the gelation time) through a control of the surface / volume ratio of the sol ( $S/V$ ). X-ray diffraction (XRD) and transmission electron microscopy (TEM) analyses of this series of samples indicated that in this way a continuous variation of the particles size can be realised, a progressive decrease of particle size with increasing  $S/V$  being observed. Unfortunately, for the samples with high  $S/V$  values, the crystalline peaks are very broad, indicating the presence of iron oxide nanoparticles at the limits of XRD observation. Moreover, the position of the main signals is consistent with the  $d$ -spacing typical for most iron hydroxides, oxyhydroxides or oxides. In [13] the presence of the *2-line* ferrihydrite phase was revealed in Fe<sub>2</sub>O<sub>3</sub> / SiO<sub>2</sub> nanocomposites, obtained by a sol gel method, through a complementary use of XRD, TEM and Mössbauer spectroscopy. In this respect it seemed very important to perform Mössbauer low temperature measurements in order to unambiguously identify the nanoparticle phase present in these composites.

Table 1. Preparation conditions of the samples.

| Composition wt% Fe <sub>2</sub> O <sub>3</sub> | Label | Volume (ml) | Surface/Volume (mm <sup>-1</sup> ) | <i>t</i> <sub>gelat.</sub> (days) | <i>T</i> <sub>calc</sub> (°C) |
|--|-------|-------------|------------------------------------|-----------------------------------|-------------------------------|
| 25   | C     | 20          | 0.037                              | 16                                | 400                           |
| 25   | B     | 7.5         | 0.100                              | 8                                 | 400                           |
| 25   | A     | 2.5         | 0.300                              | 2                                 | 400                           |

## 2. Experimental Procedure

A series of Fe<sub>2</sub>O<sub>3</sub>-SiO<sub>2</sub> nanocomposites containing 25 weight % of Fe<sub>2</sub>O<sub>3</sub> in the final product were prepared. A detailed description of the preparation, morphological and magnetic characterisation will be reported in a successive paper. In the present work, only the information essential for the understanding of the Mössbauer investigation will be given.

The starting sol was obtained by mixing TEOS (Aldrich, 98%) and an ethanolic solution of iron nitrate nonahydrate (Fe(NO<sub>3</sub>)<sub>3</sub> · 9H<sub>2</sub>O, Aldrich 98%). The hydrolysis reaction was promoted by the hydration water of the salt. The sol, with an initial acidic pH of about 1, was stirred for 15 min and then poured into three separate vessels. The vessels contained different amounts of the sol, therefore determining a variation in the surface / volume (*S/V*) ratio. The vessels were closed with a seal having a small punched hole, and then their contents was let to gel in an oven at 50 °C. The gelation time of the nanocomposites changed from 2 to 16 days for obtaining different *S/V* ratios (Table 1). The fresh gels were calcinated directly at 400 °C for 4 hours and then powdered. We investigated three samples with different *S/V* ratio; they are identified with the letters A, B and C in Table 1.

XRD powder patterns for all samples were collected between 4 to 36° of 2 $\theta$  using a Siemens D500 diffractometer with a MoK $\alpha$  radiation. TEM analysis was performed with a JEOL 200CX microscope operating at 200 kV.

Mössbauer absorption spectra were obtained in a standard transmission geometry, using a source of <sup>57</sup>Co in rhodium (370 MBq). Calibration was performed using a 25  $\mu$ m thick natural iron foil; the isomer shifts are referred to  $\alpha$ -Fe. The measurements at room temperature were carried out on powdered samples kept in a Plexiglas holder.

The measurements at low temperature were performed using a flow cryostat with Mylar windows. Nitrogen or helium were used as cryogenic liquids. These measurements were carried out using a copper

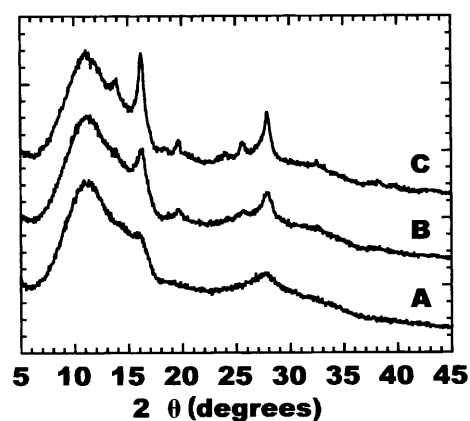


Fig. 1. XRD spectra of the three nanocomposites obtained with the preparation conditions reported in Table 1.

sample holder maintained in exchange gas (nitrogen or helium); the powders were kept between two layers of Plexiglas. The surface density of the absorber was 70, 120, and 180 mg/cm<sup>2</sup> for the sample A, B, and C, respectively.

The absorption spectra were analyzed by peaks with Lorentzian shape, using a least squares method. Actually, this fitting procedure is an approximation because superparamagnetic materials do not show simple Lorentzian line shapes, owing to the presence of phenomena of paramagnetic relaxation [14]. A quadrupole doublet was used to fit the non-blocked component, and one or two sextets were used to fit the blocked component.

## 3. Results

In Fig. 1 the XRD spectra for the three nanocomposites treated at 400 °C are reported. All the spectra show a broad halo due to amorphous silica, with a series of crystalline peaks, which are due to the iron oxide phase formed. For the sample C the diffraction peaks unequivocally indicate that the formed phase is  $\gamma$ -Fe<sub>2</sub>O<sub>3</sub>. For the other samples the peaks become broader, suggesting a progressive decrease of particle size. The particle size distribution, obtained by TEM analysis, confirms this result with average values of (6.0 $\pm$ 2.0) nm, (4.5 $\pm$ 1.5) nm and (2.5 $\pm$ 1.0) nm for the samples C, B and A, respectively. However, only on the basis of XRD results, an unequivocal identification of the iron oxide phase is not possible for the samples A and B; in particular, the spectrum of sample A is very similar to the one obtained for

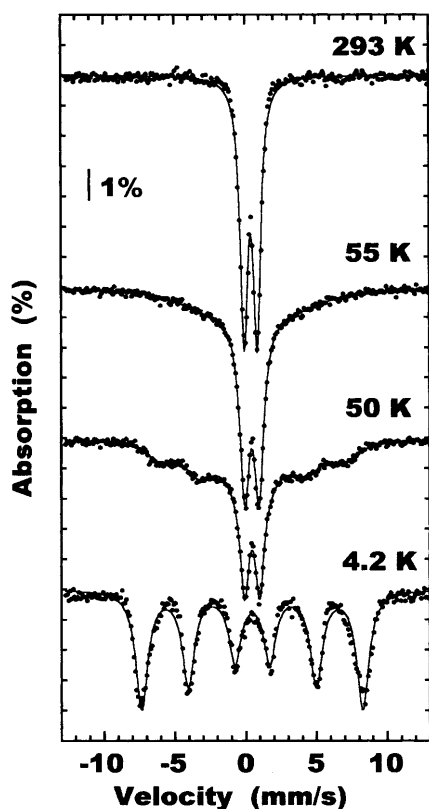


Fig. 2. Mössbauer spectra of sample A at different temperatures. The experimental points (dots) and the calculated data (solid line) are shown.

a nanocomposite containing the phase known as 2 $l$ -ferrihydrite [13].

In Figs. 2 - 4 the Mössbauer absorption spectra of the three samples, recorded at different temperatures ranging from 293 to 4.2 K, are shown. In Table 2 the results of the least squares fitting are given; the isomer shift ( $\delta$ ), quadrupole splitting ( $\Delta$ ), full width at half maximum ( $\Gamma$ ), hyperfine internal magnetic field ( $B$ ), and area ( $A$ ) of each component are reported.

Figure 2 shows the spectra of the sample A. At room temperature, only the non-blocked component can be detected. A slight appearance of the blocked component, evident as a bending of the baseline, can be observed at 55 K, but it is clearly distinguishable at 50 K.

The sample B shows a similar behaviour (Fig. 3): at room temperature only the non-blocked component is present. The blocked component can be observed at 84 K.

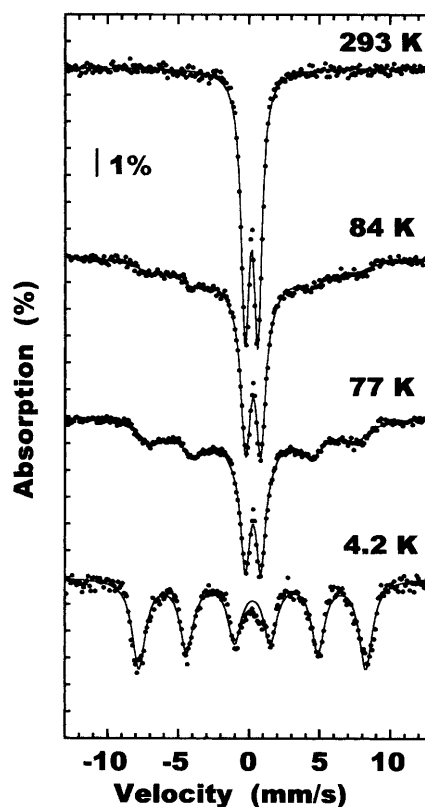


Fig. 3. Mössbauer spectra of sample B at different temperatures. The experimental points (dots) and the calculated data (solid line) are shown.

Conversely, the sample C (Fig. 4) presents a superposition of the doublet due to the non-blocked component and a Zeeman sextet due to the blocked component even in the spectrum recorded at room temperature.

At room temperature the spectra of the samples A and B show the features of paramagnetic materials. This behavior indicates that the size of the iron oxide grains is in the nanometer range. Both spectra show components with values of isomer shifts (IS) typical for trivalent iron [15, 16]; the quadrupole splitting (QS) of the superparamagnetic component is consistent with this interpretation. These spectra can be fitted by a single doublet.

Conversely, the spectrum of the sample C can be fitted with a doublet and a sextet due to a blocked state even at room temperature.

At low temperature, a superposition of the superparamagnetic component and of the Zeeman split component can be observed in the spectra of

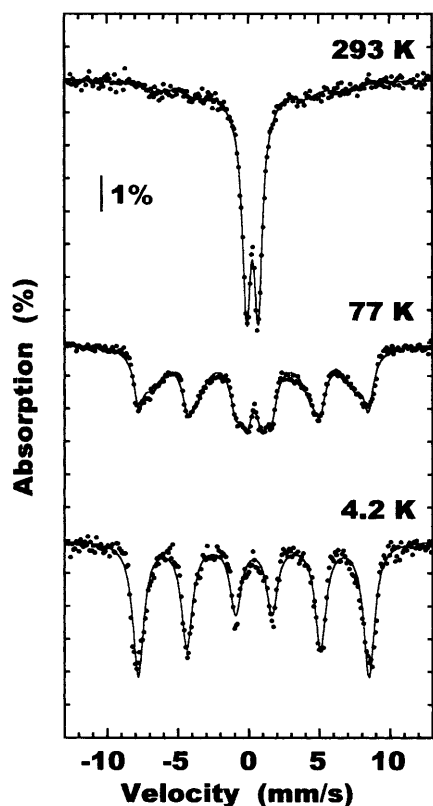


Fig. 4. Mössbauer spectra of sample C at different temperatures. The experimental points (dots) and the calculated data (solid line) are shown.

all of the three samples. This component rises as the temperature is lowered, and at liquid helium temperature the superparamagnetic doublet vanishes completely.

These spectra have been analyzed in the Lorentzian approximation, using a doublet to fit the superparamagnetic component and one or two sextets to fit the Zeeman splitted components. The broadening of the lines of the Zeeman splitted components is an effect of the size distribution of the particles; particles with different volume have a reduced magnetic field because of the effect of collective magnetic excitations [17, 18]. The area of each component is proportional to the number of iron atoms belonging to nanoparticles in the non-blocked and blocked state. The results of this fitting procedure are reported in Table 2. In the fit of the spectrum of sample C recorded at 77 K, two sextets have to be used in order to take into account the non-symmetric distribution of the values of the hyperfine field.

Table 2. Mössbauer parameters as obtained by fitting the spectra of the samples. The table shows the temperature ( $T$ ) at which the spectrum was collected, the isomer shift ( $\delta$ ), the quadrupole splitting ( $\Delta$ ), the full width at half maximum of the peaks ( $\Gamma$ ), the magnetic field ( $B$ ), and the area ( $A$ ) of each component, and statistical errors are given in parentheses as errors on the last digit.

| Sample | $T$<br>(K) | $\delta$<br>(mm/s) | $\Delta$<br>(mm/s) | $\Gamma$<br>(mm/s) | $B$<br>(T) | $A$<br>(%) | $\chi^2$ |
|--------|------------|--------------------|--------------------|--------------------|------------|------------|----------|
| A      | 293.0      | 0.34(1)            | 0.92(1)            | 0.63(1)            |            |            | 2.5      |
|        | 55.0       | 0.46(1)            | 1.00(1)            | 0.80(1)            |            | 55(1)      | 1.4      |
|        |            | 0.36(1)            |                    | 2.9(2)             | 38(1)      | 45(7)      |          |
|        | 50.0       | 0.46(1)            | 1.06(1)            | 0.74(1)            |            | 31(1)      | 1.3      |
| B      |            | 0.48(2)            |                    | 2.52(8)            | 40.0(3)    | 69(5)      |          |
|        | 4.2        | 0.47(1)            |                    | 1.04(1)            | 48.9(1)    |            | 4.6      |
|        | 293.0      | 0.33(1)            | 0.90(1)            | 0.68(1)            |            |            | 1.7      |
|        | 84.0       | 0.45(1)            | 1.07(1)            | 0.81(1)            |            | 44(1)      | 2.3      |
| C      |            | 0.43(3)            |                    | 2.9(1)             | 44.0(4)    | 56(5)      |          |
|        | 77.3       | 0.45(1)            | 1.08(1)            | 0.78(1)            |            | 33(1)      | 2.3      |
|        |            | 0.41(2)            |                    | 2.32(5)            | 44.4(2)    | 67(3)      |          |
|        | 4.2        | 0.46(1)            |                    | 1.13(2)            | 50.2(1)    |            | 3.1      |
|        | 293.0      | 0.33(1)            | 0.82(1)            | 0.68(1)            |            | 63(2)      | 1.0      |
|        |            | 0.24(8)            |                    | 2.2(2)             | 41.8(8)    | 37(8)      |          |
| C      | 77.3       | 0.46(1)            | 1.11(2)            | 0.95(2)            |            | 14(1)      | 3.3      |
|        |            | 0.42(1)            |                    | 0.74(3)            | 50.8(1)    | 25(2)      |          |
|        |            | 0.45(1)            |                    | 1.90(3)            | 44.8(2)    | 61(4)      |          |
|        | 4.2        | 0.47(1)            |                    | 0.94(2)            | 51.0(1)    |            | 3.1      |

The Mössbauer blocking temperature ( $T_{BM}$ ) is defined by the condition that the area of the blocked component equals the area of the superparamagnetic component. The  $T_{BM}$  of the samples has been calculated by using a linear interpolation or extrapolation of the relative areas in the spectra which show the two components; it was found to be  $(54 \pm 3)$  K for sample A,  $(88 \pm 6)$  K for sample B and  $(236 \pm 11)$  K for sample C.

#### 4. Discussion and Conclusions

A detailed analysis of the Mössbauer spectra, obtained in the wide range of temperatures of the three samples, on one hand confirms the results obtained with XRD, on the other hand allows to overcome the remaining ambiguity of the diffractometric study about the iron oxide phase formed.

In fact, superparamagnetic behavior is exhibited by all the samples, indicating that the size of iron oxide grains is always in the nanometer range. The decrease of the surface / volume ratio of the sol gives rise to an increase of the particles average size, while the spread of sizes around the average value increases. The size range is between that of single domain particles ( $< 10$  nm) and that of a superparamagnetic

assembly of atoms ( $\sim 1$  nm). The observed trend is clearly indicated by the evolution of the  $T_{\text{BM}}$ 's, which have the lowest values for the samples with the smallest particles, tending to maintain the superparamagnetic behavior down to low temperature.

The  $T_{\text{BM}}$  values also provide other interesting indications if compared with the blocking temperatures ( $T_{\text{max}}$ ) obtained by susceptibility measurements. The zero field cooled (ZFC) d. c. susceptibility of the sample B has been measured with a SQUID (superconducting quantum interference device) magnetometer [19]; the temperature  $T_{\text{max}}$  is 93 K [19]. For non-interacting superparamagnetic particles, the difference of  $T_{\text{BM}}$  and  $T_{\text{max}}$  is explained by the different time of measurement of the different techniques; the Mössbauer spectroscopy has a measurement time  $\tau_{\text{m}} \sim 10^{-8}$  s, which is much shorter than  $\tau_{\text{m}} \sim 100$  s of the SQUID. In the sample B the ratio between the  $T_{\text{BM}}$  and the  $T_{\text{max}}$  of the ZFC susceptibility is much smaller than that predicted by the Néel theory for non-interacting particles (ratio in the range 2-7) [20], pointing out the presence of strong interactions between nanoparticles. These results agree with TEM observations, which showed the formation of nanoparticle agglomerates along with the presence of isolated particles [19].

As regards the iron oxide phase formed, the Mössbauer investigation seems to clearly indicate that

the same phase forms in all the samples and that the phase is maghemite. The presence of a unique phase is strongly supported by the regular evolution of all the spectral parameters (consistent with the trend of XRD spectra), which do not suggest a discontinuity in the type of phase formed. As far as the phase identification is concerned, although the grain size is different, the Mössbauer spectra recorded at 4.2 K point to the formation of the ferrimagnetic  $\gamma$ -Fe<sub>2</sub>O<sub>3</sub> phase in all of the samples, also in agreement with the XRD response. In fact, the values obtained for the magnetic field  $B$  range from 48.9 T (sample A) to 51.0 T (sample C); they are typical values reported for nanocrystalline maghemite at 4 K [20] and are smaller than the value for the bulk maghemite (52.6 T) [20]; it is worthy of note that the 2-lines ferrihydrite presents smaller values of the HF (48 T) [21].

In conclusion, the Mössbauer investigation confirms that the adopted preparation method allows the formation of  $\gamma$ -Fe<sub>2</sub>O<sub>3</sub> nanoparticles with variable sizes in the range 2-6 nm, by changing the evaporation rate acting on the surface/volume ratio of the starting sol.

#### Acknowledgements

The work has been supported by MURST and CNR (Rome). We wish to thank C. Muntoni for helpful discussions.

- [1] H. Watanabe and J. Seto, *Bull. Chem. Soc. Japan* **61**, 2411 (1991).
- [2] Y. S. Kang, S. Risbud, J. F. Rabolt, and P. Stroeve, *Chem. Mater.* **8**, 2209 (1991).
- [3] R. E. Newnham, S. E. McKinstry, and H. Ikawa, *Mater. Res. Soc. Symp. Proc.* **175**, 161 (1990).
- [4] M. P. Morales, C. Pecharroman, T. Gonzales Carreno, and C. J. Serna, *J. Solid State Chem.* **108**, 158 (1994).
- [5] C. Chanéac, E. Tronc, and J. P. Jolivet, *Nanostruc. Mater.* **6**, 715 (1995).
- [6] G. Ennas, G. Marongiu, A. Musinu, A. Falqui, P. Ballirano, and R. Caminiti, *J. Mater. Res.* **14**, 1570 (1999).
- [7] R. F. Ziolo, E. P. Giannelis, B. A. Weinstein, M. P. O'Horo, B. N. Ganguly, V. Mehrotra, M. W. Russel, and D. R. Huffman, *Science* **257**, 219 (1992).
- [8] C. R. F. Lund and J. A. Dumesic, *J. Phys. Chem.* **85**, 3075 (1981).
- [9] M. H. Kryder, *MRS Bulletin* **21**, 17 (1996).
- [10] S. Onodera, H. Kondo, and T. Tawana, *MRS Bulletin* **21** (9), 35 (1996).
- [11] G. Piccaluga, A. Corrias, G. Ennas, and A. Musinu, *Material Research Foundation* **13**, 1 (2000).
- [12] F. del Monte, M. P. Morales, D. Levy, A. Fernandez, M. Ocana, A. Roig, E. Molins, K. O'Grady, and C. J. Serna, *Langmuir* **13**, 3627 (1997).
- [13] C. Cannas, G. Concas, A. Falqui, A. Musinu, G. Piccaluga, and G. Spano, *J. Non Cryst. Solids* **286**, 64 (2001).
- [14] H. H. Wickman, in: "Mössbauer Effect Methodology", Vol. 2, ed. I. J. Gruverman, Plenum Press, New York 1966, p. 39.
- [15] P. Gütlich, R. Link, and A. Trautwein, "Mössbauer Spectroscopy and Transition Metal Chemistry", Springer-Verlag, Berlin 1978, Chapt. 6.
- [16] M. Darby Dyar, *Amer. Mineral.* **70**, 304 (1985).
- [17] S. Mørup, H. Topsøe, and J. Lipka, *J. Phys.* **35** C6, 207 (1976).
- [18] L. Néel, *Ann. Geophys.* **5**, 99 (1949).
- [19] C. Cannas, M. F. Casula, G. Concas, A. Corrias, D. Gatteschi, A. Falqui, A. Musinu, C. Sangregorio, and G. Spano, *J. Mater. Chem.* **11**, 3180 (2001).
- [20] S. Mørup, F. Bodker, P. V. Hendriksen, and S. Linderoth, *Phys. Rev.* **B52**, 287 (1995).
- [21] E. Murad and J. H. Johnston, in: "Mössbauer Spectroscopy Applied to Inorganic Chemistry", Vol. 2, ed. G. J. Long, Plenum Press, New York 1987, p. 507.